Fibers, Percolation, and Spalling of High-Performance Concrete

by

Dale P. Bentz
Building and Fire Research Laboratory
National Institute of Standards and Technology
Gaithersburg, MD 20899 USA

Reprinted from American Concrete Institute (ACI) Materials Journal, Vol. 97, No. 3, 351-359, May-June 2000.

NIST
National Institute of Standards and Technology
Technology Administration, U.S. Department of Commerce

ACI MATERIALS JOURNAL TECHNICAL PAPER
Title no. 97-M41

Fibers, Percolation, and Spalling of High-Performance Concrete

by Dale P. Bentz

While the strength and durability of high-performance concretes (HPCs) are often greatly superior to conventional concretes under ambient conditions, their failure is sometimes rapid and dramatic during exposure to a fire, characterized by the explosive spalling of layers from the exposed concrete surface. This failure mode is rarely encountered in conventional concretes of higher w/c ratios. In these concretes, it is suggested that the interfacial transition zones (ITZs) surrounding each aggregate particle provide a convenient escape route for the vapor built up during the thermal exposure. In HPC, these ITZ regions are thinner and not percolated, but can be repercolated by the addition of just a few (0.2 to 0.5% by volume) fibers. Here, simulations are conducted to determine the relative efficiency of different length fibers in creating a percolated network, and to investigate the effects of aggregate volume fraction and gradation on ITZ percolation.

Keywords: concrete; fibers; high-performance concrete; spalling; water-cement ratio.

INTRODUCTION

While high-performance concrete (HPC) outperforms conventional concrete in nearly every performance category, one Achilles heel is its performance when exposed to a fire. Sporadically, such as during the recent fire in the Channel Tunnel,[1] HPC fails rapidly and dramatically due to the explosive spalling of the concrete's surface layer. This failure mode is typically not observed in conventional concretes of different mixture proportions (higher *w/c* ratio and greater volume fraction of fine aggregate) whose binder component is based solely on portland cement.[2] The mechanism of failure for HPC during a fire is not yet well understood. One possibility is that the spalling is due to the buildup of strain energy in the specimen due to thermal incompatibilities between the cement paste and aggregates.[2] During exposure to a fire, the aggregate expands, yet after an initial expansion, the cement paste actually contracts due to the loss of moisture and the generation of drying-shrinkage type stresses.[3] In HPC, the interfacial transition zones (ITZs) between aggregate and cement paste are often much denser. This could result in a higher stress concentration in the ITZ regions at elevated temperatures than in a conventional concrete where the more porous ITZ region may act as a sort of (thermal) shock absorber due to its higher porosity. While this mechanism is certainly plausible, in itself, it is somewhat difficult to reconcile with the fact that the addition of about 0.2% by volume of polypropylene fibers is able to significantly improve the fire resistance of HPC.[4] Addition of the fibers at this low volume fraction should not mitigate the thermal incompatibility problem. Furthermore, the saturation state of the concrete has been shown to affect its fire performance[5] which would be unexpected if thermal incompatibility were the sole mechanism responsible for failure.

A second hypothesis concerning the failure mechanism is that the explosive spalling is due to the buildup of very high pore pressures within the HPC. This is a result of the liquid-vapor transition of the capillary pore water, as well as that bound in the cement paste component of the concrete. An excellent review of this "moisture clog spalling" process can be found in Conzolazio et al.[6] A large portion of this water is released between 100 and 250 C when the calcium silicate hydrate (C-S-H) gel begins to degrade. This release is compounded in typical high-performance concretes due to both their higher cement factor and the presence of silica fume that produces pozzolanic C-S-H gel from the calcium hydroxide formed during hydration. A $w/c = 0.5$ cement paste with 10% silica fume can release about 50% more water in this temperature range than a reference paste with no silica fume.[7] If this water vapor cannot escape from the specimen, significant pressures will develop and may eventually cause spalling of the concrete. Recently, pore pressures on the order of 3 MPa have been measured in saturated cement mortars subjected to radiant heating.[6] Additionally, Kalifa et al.[8] have recently measured pore pressures and temperatures simultaneously inside concretes heated on one face up to 800 C, and have shown that the pressure buildup equals or slightly exceeds the saturated vapor pressure curve. In the case of saturated water vapor, pressures of 0.5, 1.5, and 3.9 MPa would be expected at temperatures of 150, 200, and 250 C, respectively.[9]

Thus, in this failure scenario, the permeability of the concrete is one critical parameter (others being the saturation state of the concrete and the heating rate) as it will regulate the rate at which the generated saturated vapor can escape from within the interior of the concrete specimen. The permeability of conventional concretes is one to two orders of magnitude higher than that of their component cement pastes.[10] Simulation studies and experimental evaluation using mercury intrusion porosimetry have indicated that this permeability increase is likely due to the percolation of the porous ITZs surrounding each aggregate particle[11] and air void.[12] Further evidence for this percolation of ITZs in conventional concretes has been provided by Wood's metal intrusion, and subsequent scanning electron microscopy evaluations of concrete by Scrivener and Nemati,[13] who suggested that the ITZ regions were indeed percolated. In addition, they estimated an ITZ thickness on the order of 20 μm in ordinary concrete, consistent with the value suggested by the concrete microstructural model employed by Winslow et al.[11]

In HPC and even in conventional *w/c* (0.45 or so) concretes containing silica fume, the thickness of the ITZ is reduced to about 10 μm or less.[14-19] In these studies, the thickness of the ITZ has been determined based on measurements of either porosity distributions using SEM analysis [15,16,18] or the orientation index of the calcium hydroxide in the ITZ and bulk paste[17,19] for *w/c* ratios ranging from 0.23 to 0.5. For a given

ACI Materials Journal, V. 97, No. 3, May-June 2000.
MS No. 99-109 received May 18, 1999, and reviewed under Institute publication policies. Pertinent discussion will be published in the March-April 2001 *ACI Materials Journal* if received by December 1, 2000.

Dale P. Bentz *is a chemical engineer in the Building Materials Division at the National Institute of Standards and Technology, Gaithersburg, Md. His research interests include fundamental, experimental, and computer modeling investigations of the hydration and microstructure of cement-based materials and the application of computer technology to building materials research.*

ITZ thickness, the volume fraction of ITZ paste is mainly dependent on the surface area of the aggregates. Thus, depending on the specific gradation and volume fraction of aggregates employed in a concrete, the ITZ regions in an HPC may or may not be percolated. This percolation concept, which subsequently will be illustrated more clearly, could thus explain the inconsistency of the performance of HPC under fire testing, as sometimes explosive spalling is observed[20] and other times not.[21] When the ITZs are themselves depercolated, the addition of polypropylene fibers (which also vaporize during the fire exposure) could perhaps provide pathways between locally percolated ITZ clusters to allow for the escape of water vapor before a significant pressure buildup produces spalling behavior. In support of this, Toutanji et al. have measured increases of up to a factor of nearly 3 in the rapid chloride permeability of concrete containing 0.3% fibers on a volume basis.[22] Furthermore, Alonso et al. have measured an increase in the room temperature gas permeability of more than three orders of magnitude, for an ultra-high-performance concrete containing fibers when first heated to 300 C relative to one heated to only 200 C. This is presumably due to the disappearance of the polypropylene fibers.[23] In this paper, a three-dimensional fiber-reinforced concrete microstructure model is presented and applied to examining the percolation of the ITZ regions in conventional and high performance concretes with and without polypropylene fibers. This study considers only the geometrical/spatial characteristics of these concretes and does not address other contributing issues such as the moisture content of the concrete or any applied load (stress state).

RESEARCH SIGNIFICANCE

As part of its Partnership for High-Performance Concrete Technology program,[24] the National Institute of Standards and Technology (NIST) is conducting research on a variety of topics critical to the performance of HPC. The fire performance of HPC is critical due to its use in high-rise building and tunnel structures. Understanding the basic mechanisms behind the spalling behavior of HPC, and the ability of polypropylene fibers to prevent spalling, is critical to the design and construction of safe and durable structures. The simulations described in this paper provide further insights into these mechanisms and can offer an approach for examining the spalling susceptibility of a concrete based on any mixture proportions of interest.

PERCOLATION THEORY

Percolation theory deals with the connectivity of components in a system. First applied by Hammersley in the 1950s,[25] an excellent introduction is provided by Stauffer and Aharony.[26] The microstructure of cement-based materials provides numerous examples of percolation phenomena.[27] Often in percolation studies, one is interested in the fraction of a phase (or phases) which is connected across the microstructure as a function of the total volume fraction of the phase(s). For example, based on observing a significant (sudden) reduction in permeability[28] as first noted by Powers, the capillary porosity in cement paste exhibits a percolation transition (from connected to disconnected) at a volume fraction of about 20% porosity, as further verified by computer simulations[29] and measurements of water imbibition during chemical shrinkage.[30,31] This transition is relatively independent of the w/c ratio, but does depend somewhat on the particle size distribution of the cement.[32] The setting of cement pastes, mortars, and concretes, illustrates the percolation of the total solids, as the individual cement particles become bonded to one-another by hydration products, leading to the formation of a percolated backbone and the strength development of the material. Other phases in the cement paste, such as the calcium hydroxide and C-S-H gel, also exhibit percolation thresholds.[29]

Once the capillary porosity depercolates, the permeability of the system is greatly reduced. In most cement pastes ($w/c \leq 0.5$), after 28 days or so, the permeability would be sufficiently low that any water vapor formed at elevated temperatures would have difficulty escaping from the system. However, in mortars and concretes, another percolation phenomena comes into play: the percolation of the ITZ regions.[11] Because the ITZ regions have a substantially larger w/c ratio than the bulk paste, they typically have a much greater (2 to 3 times) capillary porosity. Thus, if the capillary porosity in the individual ITZs remains percolated, and the ITZs themselves are percolated, a convenient escape route for the steam generated during fire exposure might exist. The percolation properties of these ITZ regions are conveniently studied using a hard-core/soft-shell (HCSS) percolation model,[33] the implementation details of which will be discussed in detail in the next section of this paper. Briefly, each aggregate particle is viewed as an impenetrable hard core, surrounded by a concentric soft shell (ITZ), which may overlap other soft shells or portions of other hard core particles. Figure 1 illustrates this HCSS model in two dimensions. In Fig. 1(a), the hard core aggregate particles are each surrounded by an ITZ region, but the ITZ regions do not percolate across the system. In Fig. 1(b), the thickness of each ITZ region has been increased such that percolation from top to bottom is achieved. In Fig. 1(c), conversely, percolation has been achieved by adding more hard-core/soft-shell particles. In Fig. 1(d), percolation is achieved by the addition of just a few fibers to the system. From this simple illustration, one can clearly see the potential efficiency of fibers in percolating the ITZ regions in an originally nonpercolated concrete. The percolation aspects of totally overlapping ellipsoids of revolution—a convenient geometrical representation of a fiber—have been simulated in detail by Garboczi et al.[34] They observed that for fibers with a 50:1 aspect ratio, approximately 1.5% by volume would be required to form a percolated pathway across a three-dimen-

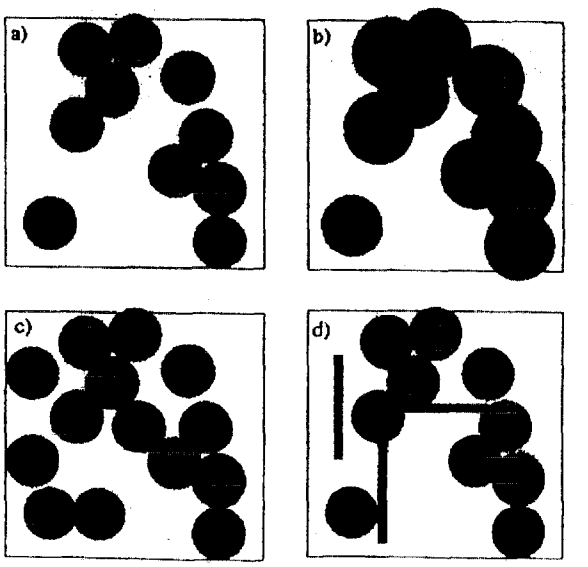

Fig. 1 Percolation of ITZs in two dimensional concrete. Hard core aggregate particles and fibers are black and soft shell ITZs are grey. Detailed description of figure provided in text.

sional microstructure. For aspect ratios of 100:1 and 200:1, this volume fraction is reduced to about 0.7 and 0.3%, respectively, suggesting that longer fibers should be more efficient in causing percolation of nonpercolated systems. This is in agreement with the rapid chloride permeability measurements of Toutanji et al., who, for concretes containing equal volume fractions of fibers, measured greater permeabilities for the systems containing longer (19 vs. 12.5 mm) fibers.[22] As a reference point, a fiber addition of 0.595 kg/m^3 (1 lb/yd^3) would correspond to approximately a fiber volume fraction of 0.06%. At this addition level, the fibers themselves should not be percolated, but could enhance the percolation of the ITZ regions surrounding each aggregate.

FIBER-REINFORCED CONCRETE MICROSTRUCTURAL MODEL

The three-dimensional microstructure of fiber-reinforced concrete is represented within the computer using the hard-core/soft-shell model. This model has recently been described in detail, [35] and software and documentation for the version of the model based entirely on spherical particles are available.* The model has been used in the past to study the chloride ion diffusivity of concrete as a function of mixture proportions,[36,37] leading to the development of an equation for estimating chloride ion diffusivity from mixture proportions and the degree of hydration of the cement.[36] The model simulates the microstructure of a cubic volume of concrete, typically 27,000 mm^3 in volume for this study. Thus, the sample is 30 mm on a side, the same scale at which spalling failures are commonly observed.[5] With a sample of this size, up to one million individual particles may be required depending on the specific aggregate gradation and volume fraction. The user specifies the particle size distribution (PSD) of the aggregates and the number of particles to place within the three-dimensional volume. The program creates a random microstructure, ensuring that no two aggregate particles overlap within the three-dimensional cubic volume. Typically, the PSD is specified via the measured sieve size classification of the aggregates. Within each sieve classification, the particle sizes are distributed uniformly by volume. For this study, the basic computer program was modified to include ellipsoidal fibers in the microstructure. Assessing the overlap of two general ellipsoids is more complex than the simple distance check that can be employed to determine if two spheres overlap. For this purpose, computer codes have been developed in the past and used to study the influence of aggregate shape on the percolation of their surrounding ITZ regions.[38] The rigid three-dimensional ellipsoids serve as a convenient computational abstraction for the polypropylene fibers, which are, in reality, deformable cylinders and may possibly bend around aggregates in the concrete.

The computer program is divided into three modules for: 1) the random placement of particles; 2) the assessment of the percolation characteristics of the surrounding ITZs; and 3) systematic point sampling to estimate the volumes of all phases (aggregates, fibers, ITZs, and bulk cement paste) in the concrete microstructure. Generally, the particles are placed from largest to smallest in size. For fibers, placement size is characterized by the largest of the three principal axis directions. For increased computational efficiency, the three-dimensional microstructure is subdivided into a set of cubic bins. This reduces the computational time required when assessing overlaps, as each particle's position need only be compared with the other particles sharing a common bin, as opposed to every other particle in the system. For the simulations presented in this paper, there were either 20 or 30 bins per dimension (8000 or 27,000 bins in the three-dimensional volume). Percolation is assessed by determining if there exists a pathway across the three-dimensional microstructure (in one principal direction) composed of the overlapping ITZ regions. All particles that are a part of this pathway are assigned a special label so that their volume fraction may be conveniently determined during the systematic point sampling. Additionally, during this sampling, a three-dimensional digital image of the microstructure (typically 150 voxels x 150 voxels x 150 voxels in size) is created in which each point is labelled as aggregate, fiber, ITZ, or bulk paste, along with its percolation state.

To examine the influence of aggregate volume fraction and gradation and fiber content on the percolation of the ITZ regions, a variety of parameters were varied in a systematic fashion. The aggregate gradations were chosen based on those designated in ASTM C 33,[39] and presented in Figure 2. The coarse aggregate followed a nominal size range of 12.5 to 4.75 mm with a maximum aggregate size of 19.0 mm. The coarse to fine aggregate ratio was fixed at a value of 1.5:1, a value typically employed in concrete mixture proportions,[4] although the influence of this ratio will be discussed in the Application to Mixture Proportioning section to follow. Aggregate volume fractions studied included 0.6, 0.65, 0.7, and 0.75 to span the range typically encountered in construction concrete. Because of the necessity of including only integer numbers of particles in the simulated concrete volume, these values varied slightly with the specific aggregate gradation being employed. Although air voids present in the concrete will behave similarly to aggregates in that each will be surrounded by an ITZ region, their influence was not examined in this study. This was based on the assumption that most of the HPC used in high-rise buildings and tunnels will not incorporate air entrainment agents. However, the computational techniques presented herein are equally applicable to air-entrained concretes, as has been demonstrated previously.[36] Recently, some evidence that air-entrained concretes may provide improved spalling resistance has been presented.[23]

For each concrete mixture proportion, the ITZ thickness was varied between 5 and 30 μm, to span the projected difference between HPCs and conventional concretes. In each case, systems with no fibers were first evaluated, and then systems with various fiber contents and geometries. Typically, fiber lengths of 10 and 20 mm were investigated and in both cases, a value of 0.25 mm was used for the fiber diameter, resulting in fiber aspect ratios of 40:1 and 80:1, respectively. For a few limited simulations, the fiber diameter was reduced to 0.1 mm to examine its effect on the percolation properties of the ITZ regions. For fiber diameters smaller than this, the diameter of the fibers would be similar to that of the original unhydrated cement particles and there would not be a well-defined ITZ region surrounding each fiber. Reducing the fiber diameter may thus reduce the volume of fibers required to achieve percolation, but there is a lower limit based on the size of the cement particles in the concrete.

All fibers were randomly oriented in the three-dimensional microstructure by generating a set of Euler angles corresponding to a random point on the surface of a unit sphere. Thus, it is being assumed that the fibers are not oriented preferentially by the concrete mixing process. Fiber contents were varied by adding different numbers (50, 75, 100, 200) of fibers to the microstructure volume to estimate the critical volume fraction needed to achieve percolation of the ITZs in those systems whose ITZ regions were originally discontinuous across the microstructure. Finally, simulations were conducted for systems containing only fibers and their ITZs, to determine their approximate percolation threshold. This value could be of particular relevance in lightweight aggregate concrete where the

*For downloading: /ftp/pub/bfrl/bentz/HCSSMODEL subdirectory at ftp.nist.gov (129.6.182.194), or available by accessing an electronic monograph at http://ciks.cbt.nist.gov/garboczi

Table 1—Minimum ITZ thickness (and volume fraction) for ITZ percolation in concrete.

Agg dist	V_{agg}=0.6	V_{agg}=0.65	V_{agg}=0.7	V_{agg}=0.75
cCcF	30 μm(0.058)	20 μm(0.042)	10 μm(0.022)	10 μm(0.024)
cCcF	30 μm(0.058)	20 μm(0.042)	10 μm(0.022)	5 μm(0.012)
cCcF	20 μm(0.038)	20 μm(0.042)	10 μm(0.022)	10 μm(0.023)
fCcF	20 μm(0.038)	20 μm(0.042)	20 μm(0.045)	5 μm(0.011)
mCmF	20 μm(0.065)	10 μm(0.032)	10 μm(0.036)	5 μm(0.018)
cCfF	10 μm(0.043)	10 μm(0.047)	5 μm(0.024)	—
fCfF	10 μm(0.042)	10 μm(0.046)	5 μm(0.024)	—

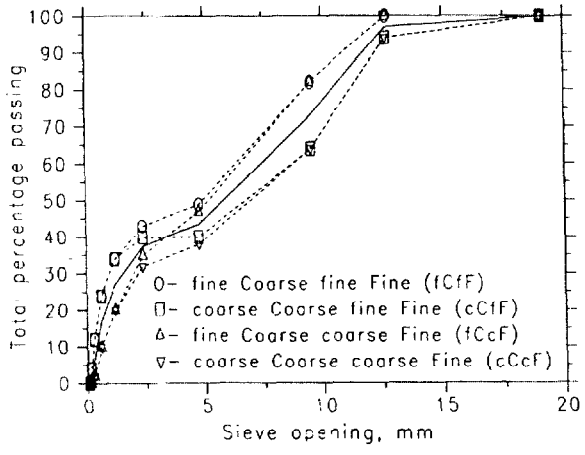

Fig. 2—Aggregate gradations examined in this study. Gradations are as indicated by symbols; central solid line indicates middle-middle (mCmF) gradation. Coarse aggregate to fine aggregate ratio is constant at 1.5:1.

ITZs surrounding aggregates may be effectively eliminated, as an ITZ denser than the bulk paste may be formed.[40,41] Indeed, Bilodeau et al.[4] have observed that a fiber content sufficient to diminish the spalling of a normal weight high strength concrete had little influence on the spalling behavior of a comparable lightweight high-strength concrete.

RESULTS

Microstructures and Percolation of ITZs

Three views of representative three-dimensional fiber-reinforced concrete microstructures are provided in Fig. 3, 4, and 5. In all three figures, the aggregate volume fraction is 0.6 (based on the cCcF distribution) and the fiber content is 0.0012, consisting of 100 fibers of length 10 mm and diameter 0.25 mm.* Figure 3 provides a simple two-dimensional surface view for two concretes with the same volume fractions of aggregates and fibers, but one based on spherical aggregates (Fig. 3a) and the other on ellipsoidal aggregates (Fig. 3b) with an aspect ratio of 1.5:1:0.6667. In Fig. 4, for simplicity, only those aggregates that are part of a percolated pathway for an ITZ thickness of 20 μm are shown in grey, with all of the fibers shown in white. Interestingly, in all three figures, one can observe that it is mainly the larger aggregates that are a part of the percolated pathway, and not the smaller aggregates that provide a major fraction of the aggregate surface area. This is illustrated quantitatively for the system with spherical aggregates in that 73% of the aggregate volume is part of the percolated pathway, while only 32% of the ITZ regions are part of this pathway. For the system with ellipsoidal aggregates, the corresponding volume fractions are 78 and 39%. Larger aggregates provide a large aggregate volume, but a proportionately smaller ITZ volume (surface area/volume ratio) than smaller ones. These results are supported by the simulations of Snyder,[42] who showed that for air voids, the probability of a given air void having a neighbor within a fixed distance was larger for the larger air voids. Correspondingly in this study, the greater surface area of an individual large aggregate makes it more likely that one of the fibers or another aggregate will intersect its ITZ volume. This finding could have a significant impact on mixture proportions for HPC as will be outlined for the case of lightweight HPC in the Application to Mixture Proportioning section to follow.

For each of the aggregate gradations examined in this study, the minimum ITZ thickness (5, 10, 20, or 30 μm) necessary to create a percolated pathway, was determined as a function of aggregate volume fraction. The results are summarized in Table 1, in which the aggregate distributions are listed from coarsest (cCcF) to finest (fCfF). For the two finest distributions, results were not generated for V_{agg} = 0.75, as well more than one million aggregates would have been required and the V_{agg} = 0.70 systems were already percolated for an ITZ thickness of 5 μm. For the cCcF distribution, three separate simulations, each using a different random number seed, were executed at each volume fraction to provide some indication of the variability due to the random configuration of the three-dimensional microstructure. From Table 1, one can clearly see that the greater the aggregate surface area (finer distributions), the lower the ITZ thickness needed to achieve percolation. In general, as would be expected, the greater the aggregate volume fraction, the lower the requisite ITZ thickness and volume fraction of ITZ paste. Since more of the concrete volume is filled with aggregates, less ITZ paste is needed to achieve percolation. For a volume fraction of aggregates of 75%, all of the distributions are percolated for an ITZ thickness of 10 μm, and one would expect that these concretes would have less propensity for spalling during a fire. However, as the volume fraction of aggregates is reduced as it typically is in HPCs,[20,21] with their higher cement content, the systems based on the coarser particle size distributions remain unpercolated for an ITZ thickness of 10 μm, and could thus be susceptible to spalling.

For those systems that are unpercolated, the addition of fibers can be extremely efficient in creating a percolated pathway. This can be observed in Figure 6 which contrasts the efficiency of adding fibers vs. adding more aggregates to a system initially containing 60% aggregates (cCcF distribution) for ITZ thicknesses of 20 and 30 μm. One can clearly observe that the fibers are nearly five times more efficient on a volume basis (0.001 addition of fibers is more or less equivalent to 0.02 addition of aggregates). This clearly illustrates the ability of the fibers to enhance the connectivity of the ITZs present in a concrete. Further illustration of the efficiency of fibers is provid

Table 2—Fiber effects on percolation properties for mCmF, V_{agg} = 0.60 concrete

Number of fibers	Fiber length (mm)	ITZ= Fiber vol. (%)	10 μm V_{AGGp}[a]	10 μm V_{ITZp}[b]	15 μm V_{AGGp}	15 μm V_{ITZp}	20 μm V_{AGGp}	20 μm V_{ITZp}
0	—	0.00	0.000	0.000	0.636	0.231	0.904	0.591
100	10	0.12	0.000	0.000	0.748	0.300	0.912	0.615
50	20	0.12	0.000	0.000	0.755	0.315	0.913	0.620
200	10	0.24	0.000	0.000	0.780	0.346	0.921	0.643
100	20	0.24	0.000	0.000	0.787	0.364	0.923	0.649
300	10	0.37	0.000	0.000	0.795	0.380	0.929	0.670
150	20	0.37	0.164	0.039	0.812	0.413	0.928	0.666

[a]Volume fraction (0–1) of total aggregates which are part of a percolated pathway.
[b]Volume fraction of all ITZ regions which are part percolated pathway.

Table 3—Fiber effects on percolation properties for mCmF, V_{agg} = 0.75 concrete.

Number of fibers	Fiber length (mm)	ITZ= Fiber vol. (%)	5 μm V_{AGGp}[a]	5 μm V_{ITZp}[b]	10 μm V_{AGGp}	10 μm V_{ITZp}
0	—	0.00	0.000	0.000	0.895	0.627
100	10	0.12	0.000	0.000	0.908	0.662
50	20	0.12	0.404	0.147	0.911	0.670
150	10	0.18	0.327	0.111	0.914	0.680
75	20	0.18	0.228	0.085	0.916	0.695
200	10	0.24	0.589	0.208	0.918	0.692
100	20	0.24	0.617	0.245	0.924	0.706

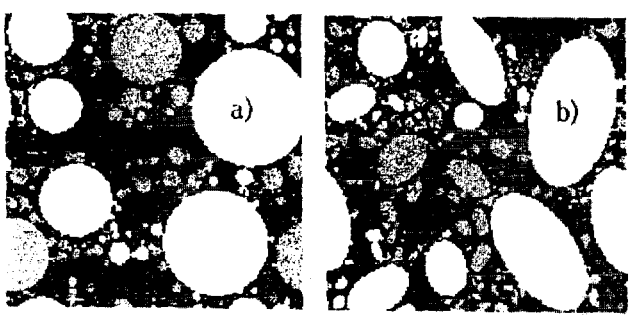

Fig. 3—Two-dimensional surface views of concrete microstructures based on (a) spherical and (b) ellipsoidal aggregates. Aggregates and fibers that are part of percolated pathway for ITZ = 20 μm (and 30 μm) are white; those that are part of pathway for ITZ = 30 μm (but not 20 μm) are light grey; other aggregates and fibers are dark grey; and bulk cement paste is black. For ellipsoidal aggregates, ratio of major to minor axis is 1.5 to 0.6667. Each image is 30 mm in each direction. Periodic boundaries are employed such that aggregate extending across one face of three-dimensional system is completed penetrating into the opposite face.

Fig. 4—View directly into face of concrete microstructure. Aggregates that are part of percolated pathway are grey, and all fibers are white. Bulk paste and nonpercolated aggregates are transparent. Image is 30 mm in each direction.

ed in Table 2 and 3. These list results for the addition of fibers to two specific concrete microstructures; one is based on the medium coarse medium fine (mCmF) distribution with 60% by volume of aggregates, and the other is based on the coarse coarse coarse fine (cCcF) distribution with V_{agg} = 0.75. For systems whose ITZ regions are unpercolated or weakly percolated, the addition of fibers is seen to significantly increase the fraction of both the aggregates (V_{AGGp}) and ITZ regions (V_{ITZp}) which are a part of the percolated network spanning the specimen. It should be noted that these volume fractions of fibers (0.1 to 0.4% by volume) correspond closely to those currently employed in structural concretes to prevent spalling.[4]

By comparing the results for the two different length fibers in Fig. 6, it can also be observed that the 20 mm length fibers (triangles) are slightly superior to the 10 mm ones (circles) in creating a percolated network. These results are also confirmed by those presented in Table 2 and 3 where in certain cases, at equivalent volume fractions, the 20 mm length fibers are able to percolate a system that remained unpercolated with

Fig. 5—Three-dimensional view of concrete microstructure with ellipsoidal aggregates. Greylevel assignments are the same as in Fig. 3. Image is 30 mm x 20 mm.

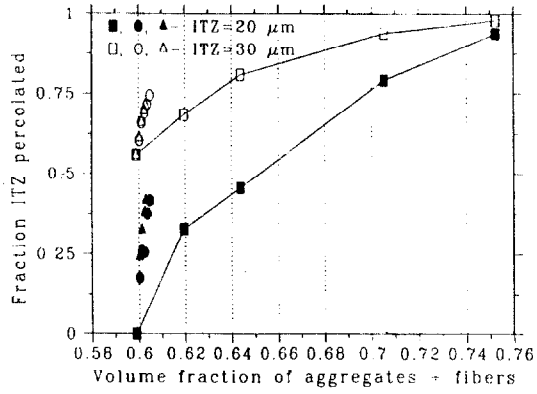

Fig. 6—Comparison of percolation efficiency of 10 mm (circles) and 20 mm (triangles) length fibers versus aggregates (squares) for cCcF aggregate gradation initially containing 60% aggregates by volume.

the addition of 10 mm fibers. In general, for the PSD distributions investigated in this study, the 20 mm fibers were slightly more efficient both in percolating an unpercolated system and in increasing the connectivity of a partially percolated one. As stated earlier, this is consistent with the percolation characteristics of totally overlapping ellipsoids.[34] For the few systems examined with the fiber diameter reduced to 0.1 mm, and the length maintained at either 10 or 20 mm for the same number of fibers, the percolated volume fractions of aggregates and ITZ regions were just slightly reduced relative to those observed for the 0.25 mm fibers. This suggests that it is the length and number of fibers that is critical in percolating the microstructure. Fibers of 0.1 mm diameter occupy only 16% of the volume of 0.25 mm diameter ones, so that the volume fraction (fiber content) needed could be significantly reduced. This must be contrasted, however, against the structural rigidity of the fiber and the fact that its diameter needs to be significantly larger than that of the cement particles in order to promote ITZ formation at the fiber-cement paste interface. The resulting fiber channel of sufficient diameter would facilitate the escape of water vapor.

For systems containing fibers only, the following percolation thresholds were observed using the computer simulation. For 10 mm length, 0.25 mm diameter fibers, volume fractions on the order of 6 and 4.5% were required for ITZ thicknesses of 20 and 30 μm, respectively. For the equivalent diameter 20 mm fibers, by contrast, the percolation thresholds were observed to be about 3 and 2.5%. For fibers of reduced diameter (0.1 mm, length = 10 mm), percolation thresholds were substantially reduced to 1.1 and 0.8% for ITZ thicknesses of 20 and 30 μm, respectively. For the 20 mm length, 0.1 mm diameter fibers, the equivalent percolation values were once again reduced by a factor of five to values of approximately 0.6 and 0.5%, respectively. All of these values are somewhat higher than those previously observed for totally overlapping ellipsoids of equivalent aspect ratios,[34] due to the restriction in the present study that the hard-core fibers can not overlap one another, although their soft-shell ITZ regions are free to overlap one another. For the 0.1 mm diameter fibers, however, the values are definitely approaching those reported earlier for the totally overlapping ellipsoid case (0.7% for an aspect ratio of 100:1, and 0.3% for 200:1). As the fibers become thinner, their ITZ regions occupy a larger proportion of their total volume and they would be expected to approach the case of totally overlapping particles, particularly for the 30 μm ITZ systems. In all cases, the longer (higher aspect ratio) fibers are seen to be the more efficient shape for creating a percolated ITZ network through a three-dimensional microstructure.

Thermal Stability of Fibers and Cement Pastes

One part of a previously proposed theory for the performance enhancement of polypropylene fibers in HPC exposed to fire is that the fibers burn out, providing a convenient escape pathway for the water vapor released during the thermal decomposition of the hydrated cement paste present in the concrete. Here, thermogravimetric analysis (TGA) will be applied to investigate this hypothesis more closely. Both the isotactic and atactic versions of polypropylene thermally decompose in the temperature range of 250 to 450 C.[43] The decomposition products are reported to be a variety of hydrocarbons, with the major components being propylene, pentene and heptene derivatives. Figure 7 provides the results of a high resolution TGA analysis, (employing a nominal scan rate of 20 C/min) of fibers from two commercial manufacturers. The results are consistent with the literature, with substantial mass loss occurring at about 250 C, and thermal decomposition being completed around 400 C.

These TGA curves can be contrasted against those obtained for the mortar components of an ordinary concrete ($w/c = 0.5$, no silica fume) and a high-performance concrete ($w/c = 0.23$, 10% condensed silica fume (CSF)), shown in Figure 8. For both concretes, a significant mass loss is observed in the temperature range of 100 to 250 C, corresponding to the loss of water from the C-S-H gel and aluminate hydration products such as ettringite.[7] For the $w/c = 0.5$ concrete, a second significant mass loss occurs in the temperature range of 450 to 550 C, corresponding to the loss of water from the calcium hydroxide (CH). Normally, a $w/c = 0.23$ cement paste would have less CH than a $w/c = 0.5$ system due to the lower degree of reaction of the cement. But with the addition of the 10% CSF, the mass loss corresponding to water in the CH is not observed at all. This is because all of the CH formed in this system has reacted with the silica fume to form pozzolanic C-S-H, which loses its water in the same temperature range as the primary C-S-H.[7] Taken together with those in Figure 7, these results suggest that when most of the water is released in a high-performance concrete, the polypropylene fibers would still be locally present in the system, and the most probable escape pathway would be through the percolated ITZ regions including those surrounding the fibers. However, two further points must be kept in mind. The first is that during exposure to a fire, a fairly sharp temperature gradient exists through the thickness of the concrete element.[7] Thus, when pressure is building at a depth of several centimeters within the concrete, the surface layer of the concrete is certainly at a temperature where the

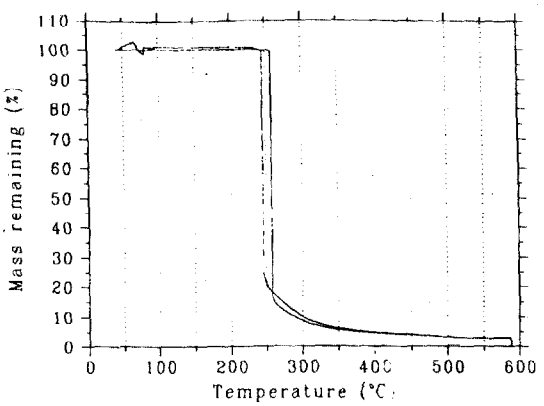

Fig. 7—Thermogravimetric analysis of fibers from two manufacturers.

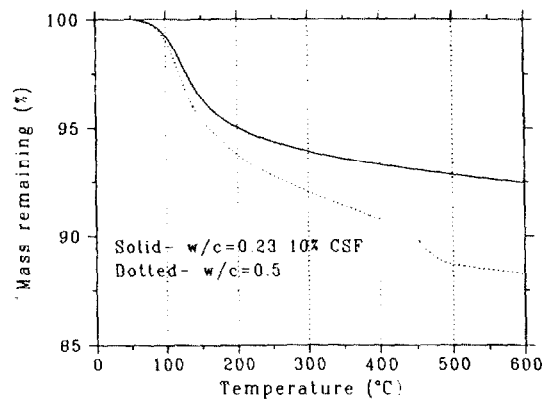

Fig. 8—Thermogravimetric analysis of two concrete mixtures.

polypropylene fibers would be completely degraded. It would be of interest to "quench" an ongoing fire test and examine the distribution of fibers as a function of depth within the concrete. Second, the polypropylene fibers do soften at around 150 C,[44] so that the possibility also exists that they are flowable and can be pushed out of the concrete, or at least locally out of the fiber channel by the exiting steam. This suggests that within a fiber-reinforced concrete exposed to a fire, there are at least three different property gradients of relevance: temperature, moisture, and fiber content.

To further investigate the fiber softening, the viscosity of the polymer melt has been measured at a temperature of 225 C, using equipment conventionally employed for measuring the flow properties of asphalts. For a shear rate of about 1.2 s^{-1}, the measured viscosity of the polymer melt was on the order of 1000 Pa-s. This is in reasonable agreement with values presented in the literature for linear low-density polyethylene,[45] where a viscosity of 8000 Pa-s was measured at a temperature of 200 C and a shear rate of 1 s^{-1}. Using this viscosity and the Hagen-Pouiselle equation for flow in a tube, one can estimate the time required for the polymer melt to flow through the fiber path (approximately cylindrical) as a function of the applied pressure. The time t to empty a fiber is given by

$$t = \frac{V_{fiber}}{Q} = \frac{8\mu L^2}{\Delta P r^2} \quad (1)$$

where V_{fiber} is the volume of the fiber; Q is the volumetric flow rate; μ is the polymer melt viscosity; L is the fiber length; r is its radius; and ΔP is the pressure drop across the fiber length.

Computer modelling[5,6] and experimental measurements[6,8] have suggested that pressures on the order of 1 to 4 MPa can be created at the depths where spalling typically occurs in a high-performance concrete exposed to a fire test. Substituting this range of values, along with the appropriate fiber geometrical parameters (L = 20 mm and r = 0.125 mm) into Eq. (1), one can calculate that between 50 and 200 s would be required for the fiber to empty. If the fiber diameter were reduced from 0.25 to 0.1 mm, this time would increase by a factor of four, according to Eq. (1). This removal time would apply for a fiber attached to the surface of the concrete. For an interior fiber, the polymer melt would also need to flow through the capillary pore system, as the fibers themselves are not percolated. Using a pore diameter of 10 μm—a conservative estimate for this calculation—one arrives at a time of 2.25 to 9 h for the polymer melt to flow a travel distance of 10 mm. These approximate calculations suggest that only those fibers in contact with the exterior surface of the concrete would be able to flow out of the concrete during a fire exposure. Because spalling often occurs at depths between 5 and 40 mm,[5] the removal of these surface fibers, due either to complete burnout or flow of the melted fibers, could substantially reduce the spalling susceptibility of an HPC exposed to fire. Conversely, those fibers whose flow path for egress includes a portion of the capillary pore network will likely remain in place, but once melted could flow into and be absorbed by the surrounding cement paste matrix. Of course, in this case, the absorbed fiber melt could also partially or totally block access to the now empty fiber channel.

To further investigate this absorption process, mortar specimens (sand/cement = 2.02, w/c = 0.36) containing 0.33 mass percent fibers per gram of cement were prepared and were subjected to constant temperature heat treatments of two hours at either 150 or 200 C. For the specimen heated to 150, the fibers basically remained intact and were readily observed in the interior of the specimens. However, for the specimen heated to 200 C, extremely few fibers were present intact after the heat treatment. The empty fiber channels, however, could be readily observed on fracture surfaces created by breaking the specimen. These empty channels, in cooperation with the ITZs, should provide a pathway for the exit of the saturated water vapor generated during the fire exposure. Since the maximum internal pressures generated within an HPC are typically characterized by a local temperature in the range of 200 to 250 C, the disappearance of the fibers at a temperature near 200 C is quite fortuitous. This observation may provide a possible explanation for the superior performance of polypropylene fibers relative to comparable additions of steel fibers which do not burnout, concerning fire performance.[5]

APPLICATION TO MIXTURE PROPORTIONING

The computer code has been designed to be applicable to any mixture proportions of interest. The user needs to specify the aggregate particle size distribution and the best set of aspect ratios to use to characterize the shape of the aggregates. The ITZ thickness will generally be controlled by the median cement particle size,[46] but will be further reduced in systems containing silica fume or other ultra-fine particles. The code could be easily extended to model a three-dimensional concrete consisting of spherical air voids, ellipsoidal aggregates, and fibers, for any mixture proportion of interest. Each particle type could have its own ITZ characteristics so that lightweight aggregates with no discernible ITZ region could be mixed with conventional aggregates and air voids with a measurable ITZ thickness. All of the studies presented in this paper have been conducted at a constant coarse aggregate to fine aggregate mass ratio of 1.5 to 1. Increasing this ratio, as is often the case when applying ACI mixture proportioning procedures for high strength concrete,[47,48] has a tendency to shift the PSD towards

the coarse-coarse, coarse-fine (cCcF) distribution, shown in Fig. 2. One example of this would be the mixture proportions employed by Sanjayan and Stocks[20] for a high-strength concrete which exhibited substantial spalling. They used a coarse aggregate to fine aggregate ratio of 2.12, as opposed to a ratio of 1.5 for their normal strength concrete, which did not exhibit spalling. This higher coarse-fine ratio would shift the PSD to the coarser region, where, as indicated by Table 1, the ITZ regions could easily be depercolated in a high-performance concrete. Conversely, Shirley et al.[21] employed ratios varying between 1.0 and 1.6, and did not observe any spalling for either normal strength or high-strength specimens. Ratios below 1.5 would tend to shift the PSD towards the fine-coarse, fine-fine (fCfF) distribution, where, as indicated by the results in Table 1, spalling would not be expected to be a problem. In this case, the ITZ regions would be expected to be percolated even for an HPC. Thus, the hypothesis developed in this paper lends support to the sporadicity of spalling observations in various research studies. Compressive strength alone is not the controlling variable, as it is the exact mixture proportions employed in each study that are of paramount importance. Likewise, the aggregate content alone is insufficient to make a spalling determination, as both aggregate volume fraction and particle size distribution are critical variables influencing the percolation of the ITZ regions. Unfortunately, the actual aggregate particle size distribution is rarely reported in studies presented in the literature.

For lightweight aggregate and ultra high-performance concretes, the ITZ regions can be effectively eliminated so that quite large concentrations of fibers (2 to 5%) may be needed to provide their own percolated pathway. In the case of lightweight aggregates, a promising compromise would be to use saturated lightweight fines along with normal weight coarse aggregates, with on the order of 0.5% by volume of fibers to percolate the coarse aggregate network. This may be viable because, as observed in Figs. 4 and 5, it is the larger aggregate particles that comprise the major portion of the percolated network, created by the addition of fibers. Additionally, the use of saturated lightweight fines will reduce self-desiccation and subsequent autogenous shrinkage, which is another Achilles heel of many HPCs.[49-52] As our basic understanding of concrete microstructure continues to develop, the potential for engineering solutions via "designer" concrete mixture proportions appears promising. The presented computational model provides a powerful tool for tailoring the exact concrete mixture proportions to the intended application.

CONCLUSIONS

A three-dimensional microstructural model for fiber-reinforced concrete has been presented and applied to examining the spalling phenomena of high-performance concrete. The hypothesis that the percolation of the ITZ regions in the concrete is of paramount importance to spalling performance, has been supported by numerous simulations and a review of documented experimental results. The efficiency of fibers to percolate a system of ITZs surrounding aggregates or increase their percolated fraction, has been clearly demonstrated. The simulation results also suggest that 20 mm fibers will provide superior performance to 10 mm ones at equivalent volume fractions. The simulations, coupled with thermogravimetric analysis of the fibers and concretes, suggest that at the temperatures where most of the water vapor is generated in a high-performance concrete, the fibers are softened and absorbed by the surrounding cement paste matrix. Measurements of the viscosity of the polymer melt indicate that while this flow within the fiber channels is possible, significant flow through the capillary pore network of the cement paste is unlikely. Thus, only those fibers in direct contact with the exterior surface are likely to be totally expelled by the pressure developing within the concrete during the fire exposure.

The developed computer program provides the opportunity to engineer a concrete with improved spalling resistance, by ensuring the percolation of the ITZ regions for the user-specified ITZ thickness. For accurate performance, the user must supply not only the aggregate volume fraction, but also the particle size distribution, based on a sieve analysis, and some insight into the specific geometrical properties (for example, aspect ratios for three-dimensional ellipsoids) of the aggregate (and fiber) particles.

ACKNOWLEDGMENTS

The author would like to thank Drs. Pierre Kalifa, Daniel Quenard, and Pierre Pimienta of Centre Scientifique et Technique du Batiment, France, for interesting discussions that stimulated this research—particularly Dr. Kalifa for the suggestion that the melting fibers could be locally absorbed by the surrounding cement matrix. The author would also like to thank Dr. Long Phan, of the Structures division of BFRL at NIST, for supplying the samples for the TGA analysis of the concretes, Mr. Robert Lutz and Mr. David Savage of the Asphalt Materials Reference Laboratory (AMRL-NIST) for assistance with the viscosity measurements, and Dr. Clarissa Ferraris and Mr. John Winpigler (BFRL) for assistance in preparing the mortar specimens containing fibers.

NOTATIONS

cCcF = coarse-coarse, coarse-fine aggregate gradation
cCfF = coarse-coarse, fine-fine aggregate gradation
CSF = condensed silica fume
C-S-H = calcium silicate hydrate
fCcF = fine-coarse, coarse-fine aggregate gradation
fCfF = fine-coarse, fine-fine aggregate gradation
HCSS = hard core/soft shell
HPC = high-performance concrete
ITZ = interfacial transition zone
L = fiber length
mCmF = middle-coarse, middle-fine aggregate gradation
PSD = particle size distribution
Q = volumetric flowrate
r = fiber radius
t = time
V_{agg} = volume fraction of aggregate
V_{AGGp} = volume fraction of total aggregates which are part of a percolated pathway
V_{fiber} = volume of a fiber
V_{ITZp} = volume fraction of all ITZ regions which are part of a percolated pathway
w/c = water to cement ratio
ΔP = pressure drop
μ = viscosity

REFERENCES

1. Demorieux, J. M., "L'incendie du Tunnel Sous la Manche. II. Diagnostic des Dommages et Inventaire des Donnees Necessaires a la Mise au Point du Projet de Reparation," *Annales du Batiment et des Travaux Publics*, Sept. 1998, pp. 43-65.

2. Phan, L. T., "Fire Performance of High-Strength Concrete: A Report of the State-of-the-Art," *NISTIR* 5934, U.S. Department of Commerce, Dec. 1996.

3. Tsimbrovska, M., "Degradation des Betons a Hautes Performances Soumis a des Temperatures Elevees: Evolution de la Permeabilite en Liaison avec la Microstructure," PhD thesis, L'Universite Joseph Fourier, 1998.

4. Bilodeau, A.; Malhotra, V. M.; and Hoff, C., "Hydrocarbon Fire Resistance of High Strength Normal Weight and Lightweight Concretes Incorporating Polypropylene Fibers," *Proceedings of the International Symposium on High-Performance and Reactive Powder Concretes*, P. C. Aitcin ed., 1998, pp. 271-296.

5. Phan, L. T.; Carino, N. J.; Duthinh, D.; and Garboczi, E. J., "International Workshop on Fire Performance of High-Strength Concrete," NIST Special Publication 919, U.S. Department of Commerce, Sept. 1997.

6. Consolazio, G. R.; McVay, M. C.; and Rish, J. W., "Measurement and Prediction of Pore Pressures in Saturated Cement Mortar Subjected to Radiant Heating," *ACI Materials Journal*, V. 95, No. 5, 1998, pp. 525-536.

7. Atlassi, E., "A Quantitative Thermogravimetric Study on the Nonevaporable Water in Mature Silica Fume Concrete," PhD thesis,

Chalmers University of Technology, Goteborg, Sweden, 1993.

8. Kalifa, P.; Menneteau, F. D.; and Quenard, D.; "Pore Pressure, Temperature, and Mass Loss in Concrete at High Temperature," paper submitted to MRS Symposium "Transport Properties and Microstructure of Cement-Based Systems," Boston, December, 1999.

9. Smith, J. M.; and Van Ness, H. C.; *Introduction to Chemical Engineering Thermodynamics*, McGraw-Hill Book Co., New York, 1975.

10. Young, J. F., "A Review of the Pore Structure of Cement Paste and Concrete and its Influence on Permeability," *Permeability of Concrete*, SP 108, D. Whiting and A. Walitt, eds., American Concrete Institute, Farmington Hills, Mich., 1988, pp. 1-18.

11. Winslow, D. N.; Cohen, M. D.; Bentz, D. P.; Snyder, K. A.; and Garboczi, E. J., "Percolation and Pore Structure in Mortars and Concretes," *Cement and Concrete Research*, 1994, pp. 25-37.

12. Rashed, A. I., and Williamson, R. B., "Microstructure of Entrained Air Voids in Concrete, Part I," *Journal of Materials Research*, V. 6, 1991, pp. 2004.

13. Scrivener, K. L., and Nemati, K. M., "The Percolation of Pore Space in the Cement Paste/Aggregate Interfacial Zone of Concrete," *Cement and Concrete Research*, V. 26, No. 1, 1996, pp. 35-40.

14. Vivekanandam, K., and Patnaikuni, I., "Transition Zone in High-Performance Concrete During Hydration," *Cement and Concrete Research*, V. 27, No. 6, 1997, pp. 817-823.

15. Scrivener, K. L.; Bentur, A.; and Pratt, P.L., "Quantitative Characterization of the Transition Zone in High-Strength Concretes," *Advances in Cement Research*, V. 1, No. 4, 1988, pp. 230-237.

16. Zayed, A. M., "The Nature of the Concrete-Steel Rebar Interface in Plain and Silica Fume Concrete," *Mat. Res. Soc. Symp. Proc.*, V. 245, 1992, pp. 341-347.

17. Monteiro, P. J. M.; Gjorv, O. E.; and Mehta, P. K., "Effect of Condensed Silica Fume on the Steel-Cement Paste Transition Zone," *Cement and Concrete Research*, V. 19, 1989, pp. 114-123.

18. Bentz, D. P.; Stutzman, P. E.; and Garboczi, E. J., "Experimental and Simulation Studies of the Interfacial Zone in Concrete," *Cement and Concrete Research*, V. 22, 1992, pp. 891-902.

19. Gjorv, O. E.; Monteiro, P. J. M.; and Mehta, P. K., "Effect of Condensed Silica Fume on the Steel-Concrete Bond," *ACI Materials Journal*, V. 87, No. 6, 1990, pp. 573-580.

20. Sanjayan, G., and Stocks, L. J., "Spalling of High-Strength Silica Fume Concrete in Fire," *ACI Materials Journal*, V. 90, No. 2, 1993, pp. 170-173.

21. Shirley, S. T.; Burg, R. G.; and Fiorato, A. E., "Fire Endurance of High-Strength Concrete Slabs," *ACI Materials Journal*, V. 85, 1988, pp. 102-108.

22. Toutanji, H.; McNeil, S.; and Bayasi, Z., "Chloride Permeability and Impact Resistance of Polypropylene-Fiber-Reinforced Silica Fume Concrete," *Cement and Concrete Research*, V. 28, No. 7, 1998, pp. 961-968.

23. Alonso, C.; Andrade, C.; and Menendez, E., "Evolucion Microestructural de Hormigones de Altas y Ultra Altas Resistences a Elevadas Temperaturas," presented at I Congreso de ACHE, Seville, Spain, Nov. 1999.

24. Frohnsdorff, G.E., "Partnership for High-Performance Concrete," *Proceedings of the International Symposium on High-Performance and Reactive Powder Concretes*, P. C. Aitcin, ed., 1998, pp. 51-57.

25. Hammersley, J. M.; Proc. Cambridge Phil. Soc., V. 53, No. 642, 1957.

26. Stauffer, D., and Aharony, A., *Introduction to Percolation Theory*, 2nd ed., Taylor and Francis, London, 1992.

27. Garboczi, E. J., and Bentz, D. P., "The Microstructure of Portland Cement-Based Materials: Computer Simulation and Percolation Theory," Mat. Res. Soc. Symp. Proc., V. 529, 1998, pp. 89-100.

28. Powers, T. C., "Capillary Continuity or Discontinuity in Cement Pastes," *PCA Bulletin*, No. 10, 1959, pp. 2-12.

29. Bentz, D. P., and Garboczi, E. J., "Percolation of Phases in a Three-Dimensional Cement Paste Microstructural Model," *Cement and Concrete Research*, V. 21, 1991, pp. 325-44.

30. Geiker, M., "Studies of Portland Cement Hydration: Measurements of Chemical Shrinkage and a Systematic Evaluation of Hydration Curves by Means of the Dispersion Model," PhD thesis, Technical University of Denmark, 1983.

31. Bentz, D.P., "Three-Dimensional Computer Simulation of Portland Cement Hydration and Microstructure Development," *Journal of the American Ceramic Society*, V. 80, No. 1, 1997, pp. 3-21.

32. Bentz, D. P.; and Haecker, C. J., "An Argument for Using Coarse Cements in High-Performance Concretes," *Cement and Concrete Research*, V. 29, No. 4, 1999, pp. 615-618.

33. Torquato, S. J., Chem. Phys., V. 85, 6248, 1986.

34. Garboczi, E. J.; Snyder, K. A.; Douglas, J. F.; and Thorpe, M. F., "Geometrical Percolation Threshold of Overlapping Ellipsoids," *Physical Review E*, V. 52, 1995, pp. 819-828.

35. Bentz, D. P.; Garboczi, E. J.; and Snyder, K. A., "A Hard-Core-Soft-Shell Microstructural Model for Studying Percolation and Transport in Three-Dimensional Composite Media," *NISTIR* 6265, U.S. Department of Commerce, 1999.

36. Bentz, D. P.; Garboczi, E. J.; and Lagergren, E. S., "Multi-Scale Microstructural Modelling of Concrete Diffusivity: Identification of Significant Variables," *Cement, Concrete, and Aggregates*, V. 20, No. 1, 1998, pp. 129-139.

37. Garboczi, E. J.; Schwartz, L. M.; and Bentz, D. P., "Modelling the Influence of the Interfacial Zone on the Conductivity and Diffusivity of Concrete," *Advanced Cement-Based Materials*, V. 2, 1995, pp.169-181.

38. Bentz, D. P.; Hwang, J. T. G.; Hagwood, C.; Garboczi, E. J.; Snyder, K. A.; Buenfeld, N.; and Scrivener, K. L., "Interfacial Zone Percolation in Concrete: Effects of Interfacial Zone Thickness and Aggregate Shape," *Mat. Res. Soc. Symp. Proc.*, V. 370, 1995 pp. 437-442.

39. ASTM C33. *Standard Specification for Concrete Aggregates, Annual Book of ASTM Standards*, Vol. 04.02, American Society for Testing and Materials, West Conshohocken, Pa., 1997.

40. Zhang, M. H.; and Gjorv, O. E., "Microstructure of the Interfacial Zone Between Lightweight Aggregate and Cement Paste," *Cement and Concrete Research*, V. 20, 1990, pp. 610-618.

41. Holm, T. A.; Bremner, T. W.; and Newman, J. B., "Lightweight Aggregate Concrete Subject to Severe Weathering," *Concrete International*, V. 6, 1984, pp. 49-54.

42. Snyder, K. A., "A Numerical Test of Air-Void Spacing Equations," *Advanced Cement-Based Materials*, V. 8, 1998, pp. 28-44.

43. Jellinek, H. H. G., ed., *Degradation and Stabilization of Polymers*, Elsevier, Amsterdam, 1983.

44. Rodriguez, F., *Principles of Polymer System*, McGraw-Hill, New York, 1982.

45. Chen, I. J.; and Bogue, D. C., "Time-Dependent Stress in Polymer Melts and Review of Viscoelastic Theory," *Transactions of the Society of Rheology*, V. 16, No. 1, 1972, pp. 59-78.

46. Bentz, D. P.; Schlangen, E.; and Garboczi, E. J., "Computer Simulations of Interfacial Zone Microstructure and its Effect on the Properties of Cement-Based Composites," *Materials Science of Concrete* IV, J.P. Skalny and S. Mindess, eds., The American Ceramic Society, Westerville, Ohio, 1995 pp. 155-199.

47. ACI Committee 211, "Guide for Selecting Proportions for High-Strength Concrete with Portland Cement and Fly Ash," 211.4R-93, American Concrete Institute, Farmington Hills, Mich., 1993.

48. Bentz, D. P.; Clifton, J. R.; and Snyder, K. A., "Predicting Service Life of Chloride-Exposed Steel-Reinforced Concrete," *Concrete International*, V. 18, No. 12, 1996.

49. Weber, S., and Reinhardt, H., "A Blend of Aggregates to Support Curing of Concrete," *Proceedings of International Symposium on Structural Lightweight Aggregate Concrete*, I. Holand, T.A. Hammer, and E. Fluge, eds., Sandefjord, Norway, 1995, pp. 662-671.

50. Bentur, A.; Igarashi, S.; and Kovler, K., "Internal Curing of High Strength Concrete to Prevent Autogenous Shrinkage and Internal Stresses by Use of Wet Lightweight Aggregates," submitted to *Cement and Concrete Research*, 1999.

51. Bentur, A.; Igarashi, S.; and Kovler, K., "Control of Autogenous Shrinkage Stresses and Cracking in High Strength Concretes," *Proceedings of 5th International Symposium on Utilization of High-Strength/Performance Concrete*, Sandefjord, Norway, 1999, pp. 1017-1026.

52. Bentz, D. P., and Snyder, K. A., "Protected Paste Volume in Concrete: Extension to Internal Curing using Saturated Lightweight Fine Aggregate," *Cement and Concrete Research*, V. 29, 1999, pp. 1863-1867.